Organic Geochemistry 161 (2021) 104315

Contents lists available at ScienceDirect

Organic Geochemistry

journal homepage: www.elsevier.com/locate/orggeochem

Targeted and untargeted lipidomic analysis of haptophyte cultures reveals novel and divergent nutrient-stress adaptations

Daniel P. Lowenstein [a,*], Kyle Mayers [b,c], Helen F. Fredricks [a], Benjamin A.S. Van Mooy [a]

[a] Department of Marine Chemistry and Geochemistry, Woods Hole Oceanographic Institution, Woods Hole, MA 02543, USA
[b] Department of Ocean & Earth Sciences, University of Southampton, Southampton, UK
[c] Molecular Ecology, NORCE Norwegian Research Centre, Bergen, Norway

ARTICLE INFO

Associate Editor—**Stefan Schouten**

Keywords:
Betaine lipids
Coccolithophore
Haptophyte
Polar lipids
Nutrient limitation
Phospholipids
Phytoplankton
Triacylglycerols

ABSTRACT

Lipids comprise a significant, highly plastic proportion of the biomass in haptophytes, a ubiquitous, globally significant, and genetically diverse clade of photosynthetic microalgae. Recent studies have investigated the cellular lipidomes of disparate, individual species of haptophytes under nutrient-replete and nutrient-limited conditions, but have not investigated how lipidomes vary across the larger evolutionary clade or its ecological functional groups. We cultured eight species of haptophytes, including five strains of *Emiliania huxleyi*, for analysis via high performance liquid chromatography–high resolution accurate mass–mass spectrometry (HPLC–HRAM–MS), and performed untargeted computational and hierarchical cluster analyses on their lipidomes. We identified similarities and differences in lipidomes along both evolutionary and ecological lines, and identified potential biomarkers for haptophyte sub-clades, including 38 glycosphingolipids, seven betaine-like lipids, and three phosphatidyl-S,S-dimethylpropanethiol (PDPT) sulfo-phospholipids. We also provide the first evidence for the glycolipid, glucuronosyldiacylglycerol, in eukaryotic microalgae. We conducted a more targeted study of four haptophyte species under nitrogen- and phosphorus-limited conditions to investigate their lipidomic responses to nutrient stress. Under N- and P-limitation, the species exhibited disparate lipidomic responses. Uniquely, in response to N-limitation, *E. huxleyi* CCMP 374 heavily upregulated PDPT from 3.6 ± 0.9% to 10.4 ± 1.5% of quantified polar lipids. These previously uncharacterized lipidomes and responses to nutrient limitation reflect divergent evolutionary strategies and challenge popular phenotypic extrapolations between species.

1. Introduction

Haptophytes are a cosmopolitan clade of eukaryotic microalgae that diverged from the larger protist community ~800 million years ago (Liu et al., 2010). There are over 750 extant, characterized species, which vary by calcification level, trophic strategy, dominant ploidy, and allelopathic potential (De Vargas et al., 2007; Guiry and Guiry, 2020). This plasticity in phenotype and life strategy has enabled haptophytes to become a dominant taxon in diverse global ecosystems (Cuvelier et al., 2010), comprising 30–50% of photosynthetic standing stock across the global ocean (Liu et al., 2009), thereby forming an important component of global primary production (Rost and Riebesell, 2004). Many species of haptophyte are capable of forming near-monospecific regional blooms with the capacity to induce meso-scale impacts on nitrogen, phosphorus, and sulfur cycling (Lessard et al., 2005; Wang et al., 2015b), and they influence the carbon cycle on both local and global scales (Rost and Riebesell, 2004; Laber et al., 2018).

A large portion of carbon in the global cycle is bound in the cellular lipidome. Wakeham et al. (1997) found 11–23% of organic carbon in marine plankton to be lipid-derived, and Bigelow et al. (2013) found lipids could compose 40–50% of dry weight in the haptophyte *Chrysochromulina* sp. More recently, Becker et al. (2018a) implicated haptophytes among the eukaryotic taxa that drive a diel lipid cycle accounting for as much as 40% of the chemical energy they capture every day from sunlight, all of which emphasizes lipids' centrality to the cycling of organic carbon and chemical energy in the ocean.

Over the last several decades, researchers have utilized lipids as biomarkers to trace biogeochemical processes throughout the ocean, including particulate organic matter production and decomposition, and various aspects of the marine nitrogen, sulfur, and trace metal cycles

* Corresponding author at: Woods Hole Oceanographic Institution, 266 Woods Hole Road, Fye 119, MS #4, Woods Hole, MA 02543, USA.
E-mail address: dlowenstein@whoi.edu (D.P. Lowenstein).

https://doi.org/10.1016/j.orggeochem.2021.104315
Received 13 March 2021; Received in revised form 5 September 2021; Accepted 6 September 2021
Available online 8 September 2021

(Wakeham and Lee, 2019; Kharbush et al., 2020; Wakeham, 2020). Early haptophyte biomarker lipid analyses focused on non-polar lipids (Nichols et al., 1991; Conte et al., 1994), and as analytical and computational sophistication has progressed, higher levels of cellular lipidomic detail and speciation have become apparent, revealing highly functional and often diagnostic/characteristic intact polar membrane lipids (Van Mooy et al., 2009; Hunter et al., 2015; Wakeham and Lee, 2019). Some of these recent breakthroughs have already contributed to a better understanding of major ocean biogeochemical cycles (Vardi et al., 2009; Becker et al., 2018a; Laber et al., 2018).

Cellular lipidomes are also highly responsive to environmental conditions, including nutrient stress, a state which is expected to predominate in large parts of the world ocean as climate change progresses (Moore et al., 2013). Early investigations of lipid remodeling found that phosphorus limitation prompts some species, including *E. huxleyi*, to replace phospholipid headgroups (e.g., phosphatidylglycerol, PG; and phosphatidylcholine, PC) with non-phosphorus headgroups (e.g., diacylglycerol carboxyhydroxymethylcholine, DGCC; and sulfoquinovosyldiacylglycerol, SQDG) (Van Mooy et al., 2009; Shemi et al., 2016).

However, despite haptophyte phenotypic and genetic diversity, and global biogeochemical significance, only a handful of species have been cultured for modern lipid analysis. Due to its preponderance in blooms and ease of culturing (Paasche, 2001; Rost and Riebesell, 2004; Beaufort et al., 2008), the coccolithophore *E. huxleyi* has been thoroughly investigated. However, while it is often held up as a model species to represent the clade (Read et al., 2013), *E. huxleyi* shows significant, fundamental phenotypic differentiation from other haptophyte species (Conte et al., 1994; Benner and Passow, 2010), and even between strains (Fulton et al., 2014; Müller et al., 2015).

Considering the "extreme [genetic] diversity" (Liu et al., 2009) in the haptophyte clade and lack of representative lipidomic studies, we sought to establish a phylogenetic framework to understand lipidomic differences and life strategies among divergent genetic lines, to identify more biomarkers to infer community structure in environmental samples, and to hopefully indicate ecologically and economically important lipids and taxa for future research. To address these goals, we cultured eight species of haptophytes, including coastal and oceanic, autotrophic and mixotrophic, calcified and non-calcified, and haploid and diploid strains for lipidomic analysis. We had three core hypotheses: (1) that we would find a haptophyte "core lipidome", an assemblage of lipid compounds shared by all species; (2) their differences would reflect either their evolutionary divergence or their ecological adaptation; and, (3) they would share similar lipid remodeling responses to nutrient stress.

Through testing these hypotheses, we have discovered previously unknown constitutive lipidomic characteristics and responses to nutrient stress in several species of haptophyte. Our work will serve as a useful starting point for more quantitative future studies.

2. Materials and methods

2.1. Culturing

Eight species of haptophyte, including five strains of *E. huxleyi*, were chosen for nutrient-replete culture studies based on phenotypic, ecological, and geographic diversity (Table 1). All species are taxonomically categorized in the class Prymnesiophyceae, according to Guiry and Guiry (2020), except where indicated (taxonomic order and replicate descriptions in parentheses and in Fig. 1). Species cultured were: haploid *Emiliania huxleyi* strain CCMP 3268 (Isochrysidales; three biological replicates), diploid *E. huxleyi* CCMP strains 370, 374, 379 (three biological replicates each), and CCMP 3266 (two biological replicates); *Haptolina ericina* CCMP 282 (Prymnesiales; two biological replicates with four technical replicates of each culture), *Isochrysis galbana* CCMP 715 (Isochrysidales; five biological replicates with three technical replicates of the last two biological replicates), *Pavlova gyrans* CCMP 608 (Class Pavlovophyceae, Order Pavlovales; three biological replicates), *Phaeocystis globosa* CCMP 628 (Phaeocystales; two biological replicates), *Phaeocystis antarctica* CCMP 3314 (Phaeocystales; three biological replicates), *Pleurochrysis carterae* CCMP 645 (Syracosphaerales; two biological replicates), and *Prymnesium parvum* CCMP 1926 (Prymnesiales; two biological replicates with three and four technical replicates of each culture; Fig. 1, Supplementary Fig. S1).

Cultures were grown in L1-Si (Guillard and Ryther, 1962) amended, 0.2 μm filtered and autoclaved, seawater in 1 L borosilicate flasks at 16–20 °C on a 12:12, light:dark cycle at 120–126 μM photons m^{-2} s^{-1} light intensity, then sampled for lipids during exponential phase. For *P. parvum*, the medium was amended with 150 μM NH_4Cl, and *Phaeocystis antarctica* was grown at 4 °C at 70 μM photons m^{-2} s^{-1} on a 14:10, light:dark cycle. To investigate lipidomic differences during different growth stages, we also analyzed one biological replicate each of *P. antarctica* and *P. globosa* in late stationary phase. Water for culture media was collected from Vineyard Sound, Woods Hole, Massachusetts, USA.

For nutrient limitation experiments, culture media were diluted to 1/25th concentration with regards to the limiting nutrient. Triplicate cultures of *E. huxleyi* CCMP 374, *I. galbana*, *P. gyrans*, and *P. parvum* were acclimated in low nutrient media for at least 5 days before being transferred to experimental flasks. They were also sampled for lipids in late exponential phase.

Algal cells were enumerated in a Sedgewick-Rafter counting chamber using a Zeiss Axiostar Plus microscope with 400× magnification (Supplementary Fig. S1). A minimum of 50 fields of view or 300 cells were counted in every sample. For cell counts greater than 10^5 ml^{-1}, a haemocytometer (Hausser Scientific, Horsham, PA, USA) was used and a minimum of 100 cells or four 1 × 1 mm^2 grids were counted. For motile species, 40 μl ml^{-1} (~4% final volume) of 8% paraformaldehyde was added to samples to inhibit movement prior to enumeration to improve accuracy. *P. antarctica* was not enumerated. Irradiance was measured using a LI-COR LI-1400 radiation sensor with a spherical probe (LI-COR,

Table 1
Algal culture species details and culture conditions.

Species	CCMP Strain	Coastal/Oceanic	Calcification	Trophic state	Media	Light:Dark (hours)	Temperature (°C)
Emiliania huxleyi	370	Oceanic	Non-calcifying	Autotrophic	L1-Si	12:12	16
Emiliania huxleyi	374	Oceanic	Non-calcifying	Autotrophic	L1-Si	12:12	16
Emiliania huxleyi	379	Oceanic	Non-calcifying	Autotrophic	L1-Si	12:12	16
Emiliania huxleyi	3266	Oceanic	Calcifying	Autotrophic	L1-Si	12:12	16
Emiliania huxleyi	3268 (haploid)	Oceanic	Non-calcifying	Autotrophic	L1-Si	12:12	16
Haptolina ericina	282	Oceanic	Non-calcifying	Mixotrophic	L1-Si	12:12	20
Isochrysis galbana	715	Coastal	Non-calcifying	Autotrophic	L1-Si	12:12	16
Pavlova gyrans	608	Coastal	Non-calcifying	Mixotrophic	L1-Si	12:12	16
Phaeocystis antarctica	3314	Oceanic	Non-calcifying	Autotrophic	L1-Si	14:10	4
Phaeocystis globosa	628	Oceanic	Non-calcifying	Autotrophic	L1-Si	12:12	16
Pleurochrysis carterae	645	Coastal	Calcifying	Autotrophic	L1-Si	12:12	16
Prymnesium parvum	1926	Coastal	Non-calcifying	Mixotrophic	L1-Si + 150 μM NH_4Cl	12:12	20

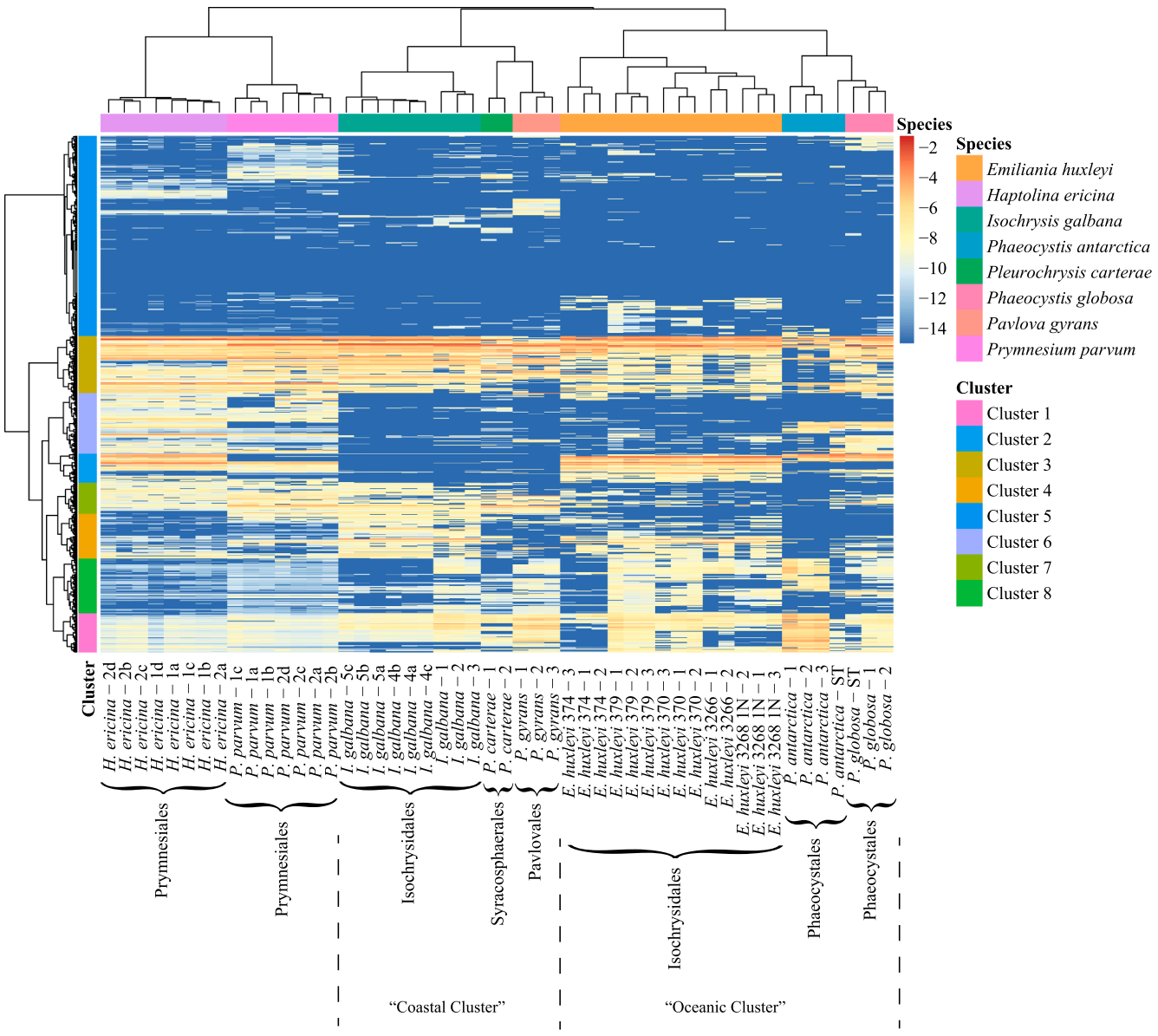

Fig. 1. Heatmap of $\log_e$-transformed proportion of total MS peak area per cell of 901 lipids identified in eight species of microalgae in five Orders (indicated in brackets) of the Haptophyta clade. All species are in Class Prymnesiophyceae, except *P. gyrans* (Class Pavlovophyceae, Order Pavlovales). Culture species (columns) and lipids (rows) are clustered based on Euclidean distance and Ward D2 minimum variance clustering. Non-detected values, i.e. $\log_e(0) = -\text{Infinity}$, were changed to a real, non-zero value one order of $\log_e$ magnitude below the lowest real value for visual clarity; heatmap with fully annotated lipids in Supplementary Fig. S2. Biological and technical replicates are indicated by number and letter after species names, respectively, except single cultures of late stationary phase *P. antarctica* and *P. globosa*, which are indicated with "ST".

Lincoln, NE, USA).

2.2. Extraction and analysis

Culture volumes ranging from 5.2 ml to 435 ml were sampled for lipid analysis (range = $2.49 \times 10^5 - 4.11 \times 10^7$ cells, mean = 7.9×10^6 cells, s.d. = 5.5×10^6 cells). Samples were vacuum filtered onto pre-combusted GF/F filters (effective pore size 0.7 μm), folded in half with sample side in, wrapped in combusted aluminum foil, flash frozen in liquid nitrogen and then stored at −80 °C until extraction. Some filters were placed into cryovials and placed at −20 °C until extraction within hours. Filters were extracted via a modified Bligh and Dyer (1959) protocol detailed in Popendorf et al. (2013), then stored at −80 °C covered in argon gas to prevent oxidation.

Extracts were analyzed via both normal- and reverse-phase high performance liquid chromatography on an Agilent 1200 HPLC system (Agilent Technologies, Santa Clara, CA, USA), with eluent gradients and chromatography columns as detailed in Sturt et al. (2004) and Collins et al. (2016). The HPLC was coupled to a Q Exactive hybrid quadrupole - orbitrap mass spectrometer (Thermo Fisher Scientific, Waltham, MA, USA). Pigments, triacylglycerols, and glycosphingolipids (GSLs) were analyzed via reverse phase chromatography, and intact polar mono- and diacylglycerol lipid classes were analyzed via normal phase. All eleven classes of intact polar lipids analyzed via normal phase were corrected for sample recovery with a dinitrophenyl-phosphatidylethanolamine (DNP-PE) internal standard and quantified using external calibration curves from authentic standards as described by Fulton et al. (2017) and, for glucuronosyl diacylglycerol (GlcADG) only, Carini et al. (2015). Lipids analyzed via reverse phase chromatography were DNP-PE recovery corrected, but were not quantified. Alkenones and sterols are not amenable to detection with our approach, but their distribution in haptophytes has been the subject of considerable prior research (e.g.,

Conte et al., 1994; Volkman, 2016).

2.3. Mass spectral identification and data analysis

Mass spectra were screened via the R-based (R Core Team, 2020) LOBSTAHS pipeline developed by Collins et al. (2016), which utilizes the ProteoWizard Toolkit (Chambers et al., 2012) for file conversion to .mzXML format, and the xcms (Smith et al., 2006; Tautenhahn et al., 2008; Benton et al., 2010) and CAMERA (Kuhl et al., 2012) packages for peak detection, grouping, retention time correction, and isotope identification.

We detected a total of 901 unique lipids within a 2.5 ppm mass certainty between 50 nutrient-replete samples and 24 nutrient-limited samples. We confirmed at least five compounds in each lipid class by ms^2 fragmentation, and identified a total of 251 lipids by ms^2 fragmentation. Nineteen of 38 total GSLs were identified by ms^2 fragmentation according to Vardi et al. (2009), Fulton et al. (2014), and Li et al. (2017). Ten TAG lipids of varying acyl lengths and degrees of unsaturation were confirmed via ms^2 according to Becker et al. (2018a). Lipid classes DGCC, PC, PG, SQDG, diacylglyceryl-trimethylhomoserine (DGTS) and diacylglyceryl-hydroxymethyltrimethyl-β-alanine (DGTA) (isomers which are indistinguishable using our methods, hereafter DGTS+DGTA), and phosphatidylethanolamine (PE) were also identified according to Becker et al. (2018a). We identified PDPT and betaine-like lipids (BLL) according to Fulton et al. (2014); GlcADG according to Carini et al. (2015) and Okazaki et al. (2013); and quinones and pigments according to Becker et al. (2018a,b) and Juin et al. (2015), respectively. Fatty acid *sn*-positions on diacyl- and triacylglycerols were not determined. Beyond the 251 lipids confirmed by ms^2 fragmentation, we identified a further 97 lipids by matching coeluting positive and negative ion mode adduct peaks, and the remaining lipids by exact mass (<2.5 ppm), adduct hierarchies (Collins et al., 2016) and retention time patterns (i.e., fewer acyl carbons decreases retention time, fewer acyl desaturations increases retention time).

All data processing and statistical analyses were performed using Thermo Xcalibur Software (Thermo Fisher Scientific, Waltham, MA, USA), RStudio (RStudio Team, 2020) and the tidyverse group of data science packages (Wickham et al., 2019).

To perform hierarchical cluster analyses on replete cultures, we first calculated a peak area fraction value for all identified lipids (i.e., peak area of each lipid divided by total peak area identified in the sample) to account for different cell sizes and counts in each culture. We then converted all lipid peak area fractions, including intact polar lipids, pigments, and neutral lipids, into log-space due to the compositional nature of relative abundance data; the optimal number of clusters was determined with the fpc package (Hennig, 2020); the pvclust package was then used to perform multiscale bootstrap resampling analyses on replete cultures (Suzuki and Shimodaira, 2015); and the pheatmap package was used to produce clustered heatmap plots (Kolde, 2019). For interspecific comparisons of pigments under nutrient replete conditions, we assumed pigments have relatively similar MS response factors to one another (Becker et al., 2021), and compared individual pigment peak area as fractions of total pigment peak area.

To assess changes in lipid class abundance in the nutrient-limitation experiments, we analyzed quantified polar lipids as mole fractions of total polar lipids to facilitate comparison between species and to account for differing cell sizes.

In assessing statistically significant differences between control and nutrient-limited treatment cultures, we chose a Benjamini and Hochberg (1995) False Discovery Rate of 0.1 because of the untargeted, exploratory nature of the experiments, after which student's t-tests were performed both for aggregated lipid classes and for all identified lipids in each experiment. Because we were not able to quantify TAG lipids, we compared the number of unique TAG molecules detected in each culture to evaluate differences between nutrient-replete and nutrient-limited treatments. We assessed differences between treatments in terms of log_2-fold change as an intuitive positive or negative "doubling" metric for relative abundance in the lipidome.

3. Results

3.1. Nutrient-replete cultures

We cultured and analyzed eight species of haptophyte, including five strains of *E. huxleyi,* in exponential growth phase under replete nutrient conditions to compare their lipidomes. We also analyzed two of these species, *P. antarctica* and *P. globosa,* in stationary phase. We identified 901 unique lipids in 50 nutrient-replete samples, including 12 intact polar lipid classes and 21 pigments. Only eleven individual lipids were detected in every nutrient-replete sample: the pigments chlorophyll *a*, chlorophyll c_2, β-carotene, diadinoxanthin, fucoxanthin, pheophytin *a*, and oxidized plastoquinone-9*;* and the glycerolipids, monogalactosyl diacylglycerol (MGDG) 32:1 (i.e., 32 acyl carbon atoms with 1 unsaturation within two acyl chains), MGDG 36:9, TAG 54:7, and TAG 58:11.

3.1.1. Hierarchical cluster analysis

We performed a 10,000-iteration multiscale bootstrap resampling analysis on all biological and technical replicates (Fig. 1) of all haptophyte species and strains, which resulted in two primary species clusters (Fig. 1, Supplementary Figs. S2 and S3). The lipidomes of both species in the order Prymnesiales, *P. parvum* and *H. ericina*, clustered together with a multiscale bootstrap resampling "Approximately Unbiased" probability-value (AU p-value) of 0.96 (Supplementary Fig. S3) (Suzuki and Shimodaira, 2015). The other main cluster was less strong (AU p = 0.70), with more defined deeper branching into two main sub-clusters: a cluster of *I. galbana, P. carterae*, and *P. gyrans*, all evolutionarily and ecologically disparate species (AU p = 0.97); and all five strains of *E. huxleyi* together with *P. antarctica* and *P. globosa* (AU p = 0.98), all predominantly open ocean species. The latter cluster further branched into *E. huxleyi* (AU p = 0.98) and both *Phaeocystis* species (AU p = 1.00). All replicates clustered within species with AU p ≥ 0.98 except late stationary phase *P. antarctica*, which clustered with *P. globosa* (AU p = 1.00). The cluster of *E. huxleyi* at the species level was also slightly less definite (AU p = 0.98), but all individual *E. huxleyi* strains clustered separately from one another (AU p ≥ 0.99).

3.1.2. Differences between nutrient-replete cultures

We observed interspecific variation in constitutive lipids among almost all major lipid classes measured. Phospholipids, predominantly phosphatidylcholine (PC) and, to a lesser extent, phosphatidylglycerol (PG), comprised 3.8 ± 1.3% to 16.6 ± 4.1% of polar lipids in oceanic species, *E, huxleyi*, *H. ericina*, *P. antarctica*, and *P. globosa*, but were only detected in trace amounts (up to 1.1 ± 0.8%) in coastal species *I. galbana*, *P. carterae*, *P. gyrans*, and *P. parvum* (Supplementary Fig. S4a; Tables 2 and 3). In contrast, betaine lipid DGCC comprised a significantly greater portion of polar lipids in the coastal species (10.2 ± 1.1% to 15.5 ± 3.4% of total polar lipids) than in the oceanic group (1.8–6.3 ± 2.3%; Supplementary Fig. S4b; Tables 2 and 3). DGTS+DGTA showed greater interspecies variation with no discernable trends (Tables 2 and 3).

Our cultures also showed intriguing presence-absence patterns of PDPT, a sulfur- and phosphorus-based diglyceride with a dimethyl sulfide (DMS) moiety in its headgroup which has been previously identified only in *E. huxleyi* (Fulton et al., 2014). PDPT constituted a roughly equivalent proportion of polar lipids in all lipidomes of *E. huxleyi* strains (3.6 ± 0.9% to 6.8 ± 0.5% of polar lipids), as well as in the *H. ericina* lipidome (5.12 ± 0.89%). It was also found in *P. parvum* at lower concentrations (1.3 ± 0.3%) and in the more closely related Isochrysidales *I. galbana* at trace levels (0.07 ± 0.02%). However, it was not detected in the distantly related *P. gyrans* or *Phaeocystis* species, nor was it detected in the coccolithophore *P. carterae* (Fig. 2; Tables 2 and 3). As in Fulton et al. (2014), we detected predominantly 22:6/14:0 fatty acid (FA) pairs

Table 2
Mole fraction of total quantified polar lipids per cell by aggregated lipid class in six species of haptophyte, including two species in late stationary phase (indicated with "ST"). Mean and standard deviation (s.d.) values in percent (%).

Lipid Class	*Haptolina ericina* (n = 8)			*Isochrisis galbana* (n = 9)			*Phaeocystis antarctica* (n = 3)			*Phaeocystis antarctica* ST (n = 1)			*Pleurochrysis carterae* (n = 2)		
	mean		*s.d.*	*mean*		*s.d.*	*Mean*		*s.d.*	*mean*		*s.d.*	*mean*		*s.d.*
DGDG [a]	19.5	±	1.77	25.6	±	2.52	14.5	±	4.96	21.0		NA	36.7	±	6.08
GlcADG	5.02	±	0.55	5.12	±	1.23	2.73	±	1.31	2.59		NA	3.09	±	0.59
MGDG+LMGDG	45.2	±	4.94	40.0	±	1.87	35.0	±	13.1	41.0		NA	34.9	±	6.92
SQDG	12.0	±	1.47	13.9	±	1.46	21.3	±	10.1	17.5		NA	10.9	±	0.29
PC	2.97	±	0.29	n.d. [b]		n.d.	14.5	±	3.44	8.14		NA	n.d.		n.d.
PE	0.26	±	0.05	n.d.		n.d.	n.d.		n.d.	n.d.		NA	n.d.		n.d.
PG	1.17	±	0.19	0.46	±	0.15	2.17	±	0.63	2.16		NA	0.64	±	0.03
BLL	0.31	±	0.08	0.21	±	0.09	0.02	±	0.01	0.17		NA	0.12	±	0.02
DGCC+LDGCC	6.12	±	0.65	11.7	±	2.35	6.32	±	2.25	3.86		NA	13.5	±	0.61
DGTS+DGTA	2.37	±	0.32	2.99	±	0.5	3.49	±	0.55	3.61		NA	0.12	±	0.07
PDPT	5.12	±	0.89	0.07	±	0.02	n.d.		n.d.	n.d.		NA	n.d.		n.d.

Lipid Class	*Phaeocystis globosa* (n = 2)			*Phaeocystis globosa* ST (n = 1)		*Pavlova gyrans* (n = 3)			*Prymnesium parvum* (n = 7)		
	mean		*s.d.*	*mean*	*s.d.*	*mean*		*s.d.*	*mean*		*s.d.*
DGDG	21.8	±	4.02	21.3	NA	37.4	±	3.56	31.6	±	5.43
GlcADG	3.48	±	0.59	2.67	NA	0.16	±	0.06	5.33	±	0.71
MGDG+LMGDG	48.2	±	3.61	47.6	NA	31.3	±	3.96	41.5	±	8.5
SQDG	13.6	±	1.52	17.5	NA	14.7	±	3.38	8.88	±	1.48
PC	6.97	±	1.63	6	NA	n.d.		n.d.	0.1	±	0.1
PE	0.06	±	0.09	0.06	NA	n.d.		n.d.	0.14	±	0.13
PG	1.32	±	0.06	1.04	NA	0.23	±	0.1	0.98	±	0.71
BLL	0.17	±	0.08	0.09	NA	0.03	±	0.06	0.07	±	0.02
DGCC+LDGCC	2.25	±	0.61	1.82	NA	15.5	±	3.42	10.2	±	1.12
DGTS+DGTA	2.09	±	0.06	1.87	NA	0.74	±	0.41	n.d.		n.d.
PDPT	n.d.		n.d.	n.d.	NA	n.d.		n.d.	1.29	±	0.26

[a]Lipid Classes: DGDG – digalactosyldiacylglycerol; GlcADG – glucuronosyldiacylglycerol; MGDG – monogalactosyldiacylglycerol; LMGDG – Lyso-monogalatosyldiacylglycerol; SQDG – sulfoquinovosyldiacylglycerol; PC – phosphatidylcholine; PE – phosphatidylethanolamine; PG – phosphatidylglycerol; BLL – betaine-like lipid; DGCC – diacylglycerylcarboxyhydroxymethylcholine; LDGCC – Lyso-diacylglycerylcarboxyhydroxymethylcholine; DGTS+DGTA - diacylglyceryl-trimethylhomoserine (DGTS) and diacylglyceryl-hydroxymethyltrimethyl-β-alanine (DGTA); PDPT – phosphatidyl-S,S-dimethylpropanethiol;
[b] n.d. – not detected.

Table 3
Mole fraction of total quantified polar lipids per cell by aggregated lipid class in five strains of *Emiliania huxleyi.* Mean and standard deviation (s.d.) values in percent (%).

Lipid Class	***E. huxleyi* CCMP 3268** (haploid; n = 3)			***E. huxleyi* CCMP 370** (n = 3)			***E. huxleyi* CCMP 374** (n = 3)			***E. huxleyi* CCMP 379** (n = 3)			***E. huxleyi* CCMP 3266** (n = 2)		
	mean		*s.d.*	*Mean*		*s.d.*	*mean*		*s.d.*	*mean*		*s.d.*	*mean*		*s.d.*
DGDG	23.7	±	1.67	20.3	±	2.19	24.1	±	6.49	26.1	±	2.41	19.1	±	0.74
GlcADG	5.53	±	0.38	5.26	±	0.71	1.61	±	0.66	5.91	±	0.08	3.20	±	1.13
MGDG+LMGDG	36.9	±	6.15	37.7	±	4.98	51.6	±	12.7	34.7	±	3.47	37.9	±	11.4
SQDG	16.8	±	5.38	18.9	±	2.19	10.8	±	2.80	19.1	±	0.28	17.9	±	9.44
PC	7.46	±	1.23	6.43	±	0.83	3.28	±	0.86	6.11	±	0.39	8.12	±	0.14
PE	n.d. [a]	±	n.d.	0.03	±	0.05	n.d.	±	n.d.	n.d.	±	n.d.	n.d.	±	n.d.
PG	0.28	±	0.34	0.57	±	0.07	0.54	±	0.41	0.30	±	0.08	0.37	±	0.15
BLL	0.84	±	0.18	0.31	±	0.06	0.15	±	0.04	0.47	±	0.15	0.44	±	0.05
DGCC+LDGCC	2.44	±	0.57	4.31	±	0.25	3.56	±	0.72	2.19	±	0.23	3.40	±	0.10
DGTS+DGTA	1.19	±	0.33	2.01	±	0.19	0.75	±	0.30	0.69	±	0.20	2.80	±	0.99
PDPT	4.83	±	0.67	4.24	±	0.47	3.55	±	0.90	4.49	±	0.36	6.82	±	0.46

[a] n.d. – not detected.

in the PDPT from *E. huxleyi* cultures, along with less abundant 22:6/16:0, 22:6/18:1 and 22:6/22:6 FA pairs in roughly equivalent amounts, although it varied between strains. Dominant PDPT FA pairs in *H. ericina* were 18:5/14:0, 18:5/16:0, 20:5/14:0 and 22:6/14:0 (Supplementary Fig. S5a).

Using the exact-mass theoretical lipid database generation built into the LOBSTAHS R-based lipidomics package (Collins et al., 2016), and confirming with ms/ms fragmentation, we identified a series of novel GSLs that show potential as biomarkers for individual haptophyte species, similar to hGSL in *E. huxleyi* (Vardi et al., 2012). We detected a range of GSLs in every species at varying levels of expression, with species-specific long chain bases (LCBs) and FAs of various lengths and degrees of unsaturation. We observed only dihydroxy-LCBs paired with monohydroxy-FAs (Supplementary Table S1). Lower molecular weight (<750 Da) GSLs were found exclusively in *P. gyrans*, with a trace-level exception in *P. parvum*. Medium-low *m/z* (750–780 Da) GSLs were predominant in *H. ericina*, *P. globosa*, and *P. gyrans*. Medium-high *m/z* GSLs (780–810 Da) were primarily found in *I. galbana*, *P. gyrans*, *Phaeocystis* spp. and all strains of *E. huxleyi*. High *m/z* GSLs (810–850 Da) predominated in *P. carterae* and *P. parvum* cultures. Only trace GSLs were detected in exponential phase *P. antarctica* (Table 2, Supplementary Table S1), possibly due to low filtered cell counts. *E. huxleyi* CCMP 379 and haploid *E. huxleyi* CCMP 3268 produced the largest range of unique LCB/FA pairs, with 14 and 13 pairs detected above trace levels, respectively. In contrast, late-stationary phase *P. antarctica* produced the lowest GSL diversity, with only two compounds detected above trace levels (Supplementary Table S1).

Sialic acid GSL (sGSL), a lipid previously connected with *E. huxleyi*

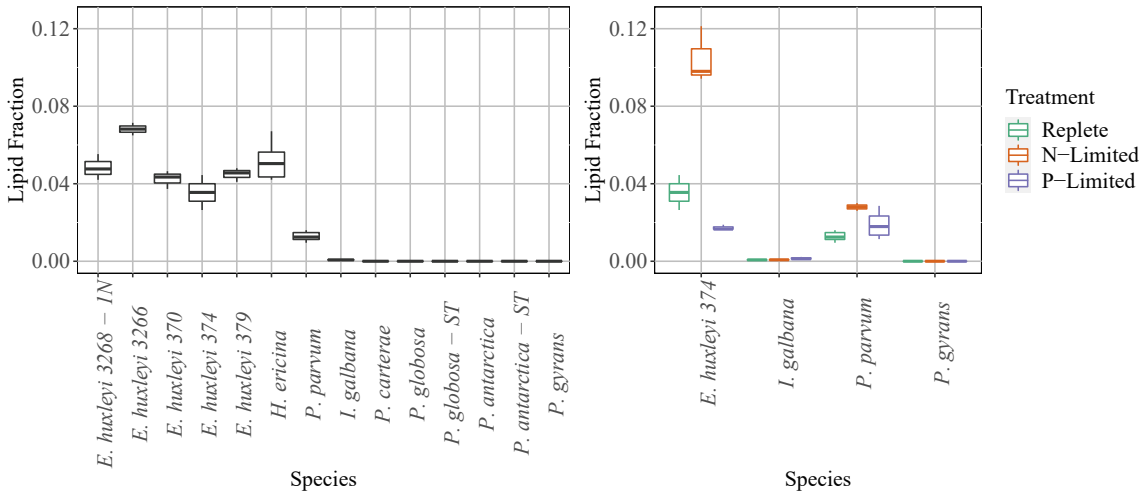

Fig. 2. Sulfo-phospholipid, phosphatidyl-S,S-dimethylpropanethiol (PDPT), expressed as a mole fraction of total quantified polar lipids in eight haptophyte microalgae species under nutrient-replete conditions (a) and four species in nutrient-replete, and N- and P-limited media (b). Box lines indicate first quartile, median, and third quartile; whiskers indicate minimum and maximum values.

susceptibility to viral infection (Fulton et al., 2014; Hunter et al., 2015), was only detected in *E. huxleyi*. Concordant with these previous studies, sGSL was not detected in the haploid culture or the virus-resistant strain CCMP 379 (Supplementary Table S1).

Another polar lipid previously reported only in haptophytes is BLL, which was first identified by Fulton et al. (2014) and has thus far eluded complete structural characterization. BLL was detected in all species (<1% of polar lipids) (Supplementary Fig. S4c; Tables 2 and 3) with potentially diagnostic species-specific fatty acid pairs (Supplementary Fig. S5b). *I. galbana* produced only BLL 22:5/16:0 above trace levels. In *P. carterae* cultures, we detected only BLL 22:6/18:0 and BLL 22:5/18:0. All strains of *E. huxleyi* predominated in BLL 22:6/16:0 and BLL 22:6/18:1, with minimal BLL 22:6/18:0. All of the Prymnesiales and Phaeocystales species (i.e., *P. parvum*, *H. ericina*, *P. antarctica,* and *P. globosa*) expressed BLL 22:6/22:6, a lipid previously only detected in abundance in virally infected *E. huxleyi* (Fulton et al., 2014; Hunter et al., 2015). *P. gyrans* only produced BLL 22:6/18:1. Among *E. huxleyi* cultures, BLL constituted a significantly greater proportion of the haploid lipidome than in any diploid strain (Supplementary Fig. S4c; Table 3).

GlcADG, a glycolipid associated with phosphorus stress response in higher plants (Okazaki et al., 2013) and some marine heterotrophic bacteria (Carini et al., 2015; Sebastián et al., 2016) was detected with distinct dominant fatty acid pairs in all cultured species (1.6 ± 0.7% to 5.9 ± 0.08% total polar lipids; Supplementary Fig. S5c; Tables 2 and 3) except *P. gyrans,* where it was detected only at trace levels (0.16 ± 0.06%, Table 2). The GlcADG signal in *E. huxleyi* and *I. galbana* was dominated by the fatty acid pair 18:1/14:0. GlcADG 18:1/16:0 was also a major ion in *I. galbana*. *P. carterae* cultures contained predominantly GlcADG 18:1/16:0 and GlcADG 18:2/16:0. The dominant peak in both *H. ericina* and *P. parvum* was GlcADG 22:6/16:0. *P. antarctica* and *P. globosa* both had two dominant ions, GlcADG 22:6/16:0 and 18:1/14:0 (Supplementary Fig. S5c).

We detected interspecific variations in various pigments, generally in agreement with landmark haptophyte pigment analyses by Zapata et al. (2004). Frequent haptophyte biomarker pigments, 19′-hexanoyloxyfucoxanthin and 19'-butanoyloxyfucoxanthin, were detected only in *E. huxleyi*, *H. ericina, P. antarctica,* and *P. globosa*, while chlorophyll c_1 was only detected in *I. galbana, P. carterae, P. gyrans,* and *P. parvum* (Supplementary Tables S2 and S3). We detected a wide range of total plastoquinone abundance, with peak area ranging from 0.3 ± 0.04% of total pigment peak area in *H. ericina* to 4.9 ± 0.9% in the haploid *E. huxleyi* strain 3268. We also detected wide ranges in β-carotene peak area among species and strains, with proportions between ~0.05% in *P. parvum* to over 5% of detected pigment peak area in *P. globosa*, and a range of 3.6 ± 0.2% to over 22% of total pigment peak area among strains of *E. huxleyi* (Supplementary Tables S2 and S3).

3.2. Nutrient stress

We subjected a subset of the cultures, *E. huxleyi* CCMP 374*, I. galbana, P. gyrans* and *P. parvum*, to N- and P-limitation to investigate how they remodeled their lipidomes to cope with the nutrient stress. We found that each species responded differently to both N- and P-limitation, with some commonalities (Fig. 3, Supplementary Fig. S2b; Table 4, Supplementary Tables S4, S5, and S6). Importantly, we noted that dominant FA and LCB pairs of potential biomarker molecules (i.e., BLL and GSL) did not change under nutrient stress.

3.2.1. Nitrogen stress

In response to N-limitation, *E. huxleyi*, *I. galbana,* and *P. parvum* all showed significant changes in relative abundance of at least 10% of polar lipids detected under replete conditions (11–69%; Fig. 3, Supplementary Fig. S2b; Supplementary Table S4). In all three species, we detected a significantly greater number of unique TAG lipids than under nutrient-replete conditions (Supplementary Table S5). In N-limited *E. huxleyi*, we detected 54 ± 6 unique TAGs, increased from 24 ± 3 unique TAGs under nutrient-replete conditions ($p = 6.5 \times 10^{-3}$); in N-limited *I. galbana*, we detected 139 ± 7 unique TAGS, vs 93 ± 30 in the control ($p = 1.8 \times 10^{-3}$); and we identified the greatest TAG molecular diversity in N-limited *P. parvum*, with 223 ± 1 unique TAGs compared to 161 ± 8 in the nutrient-replete cultures ($p < 0.001$).

E. huxleyi, I. galbana, and *P. parvum* all showed significant changes to the segments of their lipidome devoted to photosynthesis. The thylakoid membrane lipid SQDG decreased −0.43 $\log_2$-fold in *P. parvum* ($p = 0.006$) and −0.65 $\log_2$-fold in *I. galbana* ($p = 2.7 \times 10^{-3}$; Table 4). However, digalactosyldiacylglycerol (DGDG) decreased in relative abundance in *P. parvum* (−0.44 $\log_2$-fold, $p = 0.007$), while MGDG increased in *I. galbana* from 40.0 ± 1.9% to 51.3 ± 2.1% of polar lipids ($p = 2.8 \times 10^{-3}$). GlcADG more than doubled in relative abundance in N-stressed *E. huxleyi*, from 1.6 ± 0.7% to 3.8 ± 0.9% ($p = 0.034$), but decreased from 5.1 ± 1.2% to 3.7 ± 0.3% in *I. galbana* ($p = 0.01$).

P. parvum showed the greatest reduction to its non-glycolipid reservoir, with its most prominent betaine lipid class, DGCC, exhibiting a −0.93 $\log_2$-fold change to comprise 5.3 ± 0.7% of polar lipids ($p = 7.0 \times 10^{-3}$, Table 4).

Uniquely among all cultured species under N-stress, *E. huxleyi*

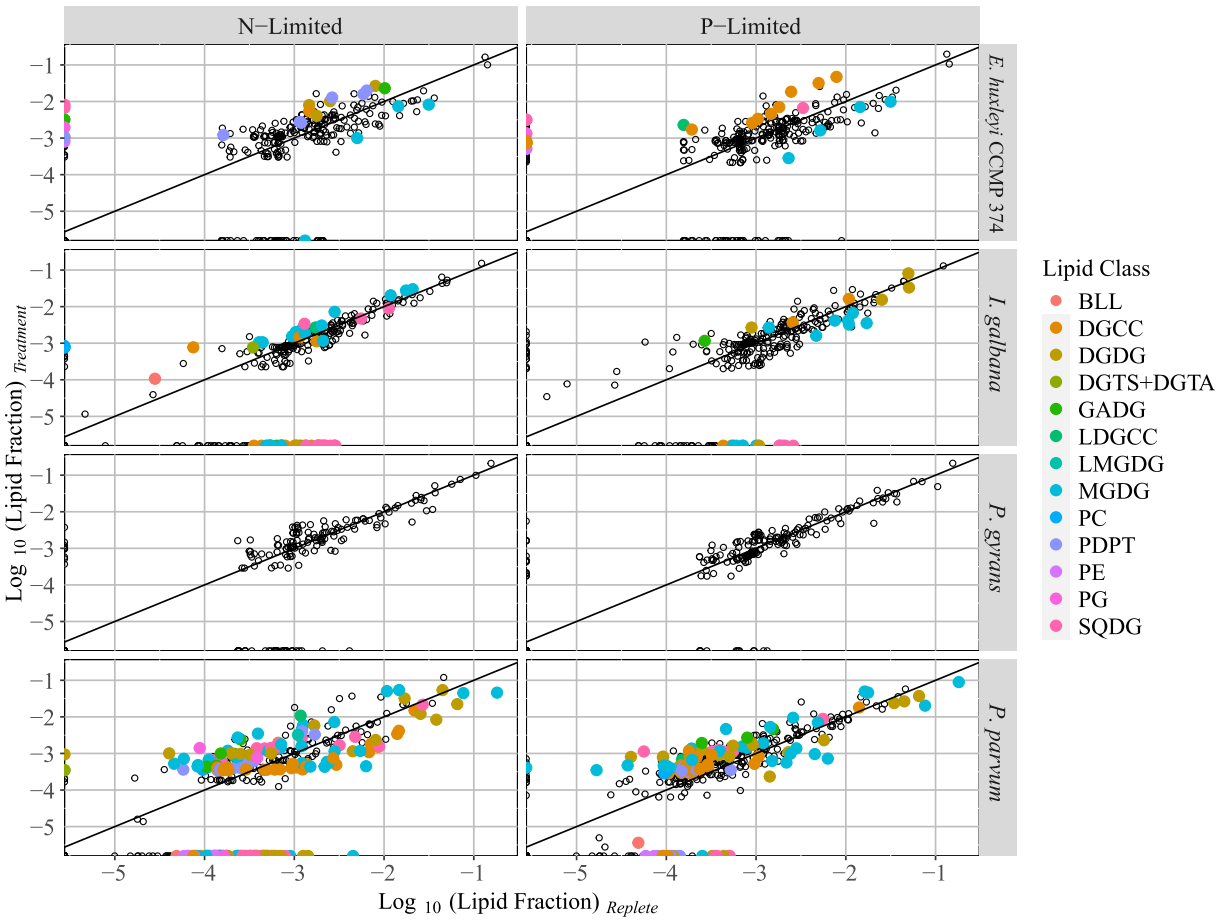

Fig. 3. Individual lipid expression as log_{10}-transformed mole fraction of total quantified polar lipids in four species of haptophyte under nutrient-replete, and N- and P-limited nutrient conditions. Solid data points, colored by lipid class, indicate Benjamini-Hochberg FDR-controlled significant differences; hollow points indicate nonsignificant differences. Diagonal line indicates 1:1, $mean_{replete}$: $mean_{treatment}$ lipid mole fraction.

Table 4
Significant log_2-fold changes in mole fraction of polar lipid classes between Replete and N- or P-limited cultures of *E. huxleyi* CCMP 374, *Isochrysis galbana*, *Pavlova gyrans*, and *Prymnesium parvum*. Mean and standard deviation (s.d.) values in percent (%). Non-significant changes are not shown but are available in Supplementary Table S6.

		Replete		N-Limited				P-Limited			
Species	**Lipid**	**Mean**	**SD**	**Mean**	**SD**	**Log_2 Fold Change**	**p-value**	**Mean**	**SD**	**Log_2 Fold Change**	**p-value**
***E. huxleyi* CCMP 374**	GlcADG	1.61	± 0.66	3.81	± 0.93	1.24	0.034				
	PDPT	3.55	± 0.90	10.4	± 1.50	1.56	4.36E−03				
	DGCC+LDGCC	3.56	± 0.72	6.13	± 0.67	0.78	0.011	15.1	± 0.81	2.09	5.54E−05
	PE	n.d. [a]	n.d.	0.08	± 0.01	Inf	3.57E−03	0.27	± 0.06	Inf	0.018
	BLL	0.15	± 0.04					0.26	± 0.02	0.77	0.035
	SQDG	10.8	± 2.80					19.2	± 3.20	0.83	0.027
I. galbana	GlcADG	5.12	± 1.20	3.68	± 0.32	−0.47	0.01				
	MGDG+LMGDG	40.0	± 1.90	51.3	± 2.10	0.36	2.76E−03				
	SQDG	13.9	± 1.50	8.84	± 1.20	−0.65	2.72E−03				
	PC	n.d.	± n.d.	0.24	± 0.03	Inf	4.62E−03				
	DGCC+LDGCC	11.7	± 2.40					15.0	± 1.30	0.36	0.017
	DGDG	25.6	± 2.50					29.5	± 1.00	0.21	3.71E−03
P. gyrans	PC	n.d.	± n.d.	0.40	± 0.05	Inf	6.00E−03				
	PG	0.24	± 0.10	0.73	± 0.17	1.63	0.02				
P. parvum	BLL	0.08	± 0.02	0.20	± 0.01	1.41	5.73E−05				
	DGDG	31.6	± 5.40	23.3	± 0.39	−0.44	7.00E−03				
	PDPT	1.29	± 0.26	2.80	± 0.28	1.12	0.041				
	PE	0.14	± 0.13	0.01	± 0.02	−3.52	0.038				
	SQDG	8.88	± 1.50	6.58	± 0.21	−0.43	6.00E−03				
	DGCC+LDGCC	10.2	± 1.10	5.32	± 0.70	−0.93	7.00E−03	12.9	± 1.40	0.35	0.016
	GlcADG	5.33	± 0.71					7.84	± 1.20	0.56	0.017

[a] n.d. – not detected.

expressed a significant 1.56 log_2-fold increase in relative abundance of PDPT (Fig. 2), up to over 10% of polar lipids in the N-limited cultures ($p = 4.4 \times 10^{-3}$, Table 4). Interestingly, DGCC also increased in relative abundance from 3.6 ± 0.8% to 6.1 ± 0.7% of polar lipids ($p = 0.011$). *P. parvum* also showed increased relative abundance of PDPT, up to 2.8 ± 0.3% of polar lipids.

In contrast, *P. gyrans* did not show significant changes in relative expression of any individual polar lipid. Though PC was not detected in nutrient-replete *I. galbana* or *P. gyrans*, we detected trace levels of PC in both N-limited cultures (Table 4).

3.2.2. Phosphorus stress

Under P-limitation, each cultured species exhibited a similarly mixed response, but with fewer significant changes than under N-limitation (Supplementary Fig. S2b; Table 4, Supplementary Table S4). In *E. huxleyi, I. galbana*, and *P. parvum,* we measured significant increases in total DGCC and Lyso-DGCC, up to 15.1 ± 0.8% of polar lipids in *E. huxleyi* ($p < 0.001$), 15.0 ± 1.3% in *I. galbana* ($p = 0.017$), and 12.9 ± 1.4% in *P. parvum* ($p = 0.016$; Table 4). In *E. huxleyi*, we observed an almost two-fold increase in SQDG to 19.2 ± 3.2% of all polar lipids ($p = 0.027$), and an increase of DGDG to 29.5 ± 1.0% in *I. galbana* ($p = 3.7 \times 10^{-3}$, Table 4). We also measured an increase of GlcADG in *P. parvum*, to 7.8 ± 1.2% ($p = 0.017$). Only *I. galbana* produced a significantly greater number of unique TAG lipids under P-limitation (145 ± 14 detected TAG lipids) than under nutrient-replete conditions (93 ± 30 detected lipids; $p = 3.8 \times 10^{-3}$; Supplementary Table S5).

Previous studies applied ratios of non-phosphorus polar lipids to phospholipids to diagnose P-limitation in the ocean (Van Mooy et al., 2009; Martin et al., 2014). We found evidence for this phenomenon in the zwitterionic substitution pair (total DGCC:PC), in which *E. huxleyi* showed an increase in its log_{10}(DGCC:PC) ratio from −0.029 to 0.69 ($p < 0.001$; Supplementary Fig. S6a), but ratios in *I. galbana, P. gyrans, and P. parvum* were confounded by the absence of detectable PC in replete cultures. Interestingly, no species showed significant changes in the ratio of the anionic chloroplast lipids, SQDG and PG (Supplementary Fig. S6b).

As under N-limitation, *P. gyrans* showed no significant changes in relative abundance of any individual polar lipid under P-limited conditions (Fig. 3; Supplementary Table S4), nor did any aggregated lipid class show changes in relative abundance (Table 4, Supplementary Table S6).

4. Discussion

The aim of this study was to determine whether the haptophyte clade had conserved lipidomes and nutrient-limitation remodeling strategies, or whether evolutionary divergence had resulted in unique lipidomes and stress responses. We revealed a minor conserved “core lipidome”, a group of lipids expressed by all species we studied. This affirmed our first hypothesis. However, this core was surprisingly small, consisting of only eleven lipids: seven pigments, two TAG lipids, and two MGDG lipids. Instead, we discovered expansive, unique lipidomes among the different haptophyte species, with varying levels, and potentially diagnostic presence and absence, of the vast majority of the observed lipids.

4.1. Hierarchical cluster analysis

Under nutrient-replete conditions, hierarchical cluster analyses of all the haptophyte species and *E. huxleyi* strains shows consistent clustering within the genus. However, above the genus level, the replete lipidomes clustered in a manner inconsistent with phylogenetic trees based on 18S and molecular clock analyses (Fig. 1, Supplementary Figs. S2 and S3; Medlin et al., 2008; Liu et al., 2010; Edvardsen et al., 2011). This suggests that recent ecological adaptations have had a more significant effect on cellular lipidomes than overall selective pressures and species differentiation over the last ~800 million years, as reflected in ribosomal RNA phylogeny.

Our cluster analysis shows primary branches separating into three major groups: all strains of *E. huxleyi* and both *Phaeocystis* species in one cluster; Prymnesiales *H. ericina* and *P. parvum* in another; and phylogenetically distant *I. galbana*, *P. carterae,* and *P. gyrans* in the other. All three clusters were strongly supported by the data (AU p-values > 0.96).

The oceanic, bloom-forming *E. huxleyi* and *Phaeocystis* cluster was primarily characterized by expression of the membrane phospholipid, PC, while the coastal cluster of *I. galbana*, *P. carterae,* and *P. gyrans* was characterized by higher levels of the typical haptophyte betaine lipid, DGCC, and < 1% phospholipids. Similar betaine and phospholipid levels were found by Cañavate et al. (2017a) in *I. galbana* and Pavlovales *Diacronema vlkianum*. The two clusters also diverged along presence-absence of the oceanic 19'-fucoxanthins and coastal chlorophyll c_1 (Supplementary Tables S2 and S3). Notably, late-stationary phase *P. antarctica* clustered closer to exponential phase *P. globosa* than to exponential phase *P. antarctica*, reflecting the extreme similarity of the species' lipidomes.

The non-calcifying Prymnesiales, *H. ericina* and *P. parvum*, composed their own cluster exhibiting shared and distinct lipidomic characteristics from both other clusters. Both species contained DGCC in significant abundance, with *P. parvum* at an equivalent level to the coastal cluster and *H. ericina* at roughly half that, but both contained significant levels of phospholipids PC and PDPT, which were almost undetected in the coastal cluster. However, *H. ericina* expressed both PC and PDPT at much greater levels than *P. parvum*, more akin to the oceanic cluster. Finally, the two also exhibited the coastal-oceanic divide in biomarker pigments, with *H. ericina* expressing only the 19'-fucoxanthins and *P. parvum* only chlorophyll c_1 (Supplementary Table S2).

The observed headgroup stoichiometry strategies of these eight species, separable along coastal-oceanic lines, could help explain regional species predominance in the world ocean and its estuaries. Increased nitrogen loading into estuaries and coastal seas in the recent geological past (Vitousek et al., 1997) may have selected for species with high environmental N:P requirements, like *Isochrysis* affinis *galbana* (Marchetti et al., 2012), while N-limited open oceans see species like *E. huxleyi* thrive (Lessard et al., 2005). This understanding may also help predict how phytoplankton community structures will respond to future changes in ocean chemistry and resource availability.

At large, our findings suggest haptophyte lipidomes are more likely to reflect ecological niche and regional macronutrient availability than their ancestry.

4.1.1. Potential biomarkers

In the last decade, GSLs have become powerful indicators of *E. huxleyi* blooms, viral susceptibility, and state of infection (Vardi et al., 2012; Hunter et al., 2015; Laber et al., 2018), and other sphingolipids have been identified across clades of marine microalgae (Ray et al., 2014; Li et al., 2017). GSLs have been associated with lipid rafts and microdomains for functional proteins, including nutrient transporters, in *E. huxleyi* (Rose et al., 2014) and other organisms from bacteria to humans (Hakomori, 2008). Their apparent phylogenetic specificity makes them ideal biomarkers to trace biological activity and biogeochemical inputs.

With the benefit of advances in our lipid database generation and automated MS screening capabilities, we discovered a diverse range of GSLs spread across the clade (Supplementary Table S1), serving as evidence of probable ubiquity in haptophytes (Fulton et al., 2014; Hunter et al., 2015). Our findings agree with Li et al. (2017) who found unique LCB/FA pairs and glycosyl moieties among selected haptophytes, diatoms, and dinoflagellates. However, we detected a greater diversity of LCB/FA pairs in each species than previously seen, as well as enough species- and habitat-specificity for GSLs to serve as potential environmental biomarkers, especially given their apparent stability through nutrient limitation. However, it should be noted that virus-infected *E. huxleyi* does show some changes in individual GSL abundance

(Hunter et al., 2015). Compounds most closely associated with *E. huxleyi*, hGSL and sGSL, appear to remain good biomarkers for open-ocean *E. huxleyi* blooms (Supplementary Table S1). Interestingly, sGSL was absent in *P. parvum* despite the recent discovery of sialic acid synthesis in this organism (Wagstaff et al., 2018).

Since the first identification of BLL in a study of virus infection in *E. huxleyi* (Fulton et al., 2014), then its subsequent application as a biomarker in the North Atlantic (Laber et al., 2018), BLL has only been identified in two other organisms, also haptophytes, *Isochrysis* sp. CCMP 1324 and *Phaeocystis pouchetii* (Fulton et al., 2017). Our results suggest that BLL is likely distributed across the Haptophyta phylum. Both its broader physiological function and the more nuanced species- and strain-specific differences in fatty acid composition will require more research, as will efforts to investigate it outside the haptophyte clade. Though characteristic FA pairs appear to remain constant through nutrient stress, at the minimum, the data presented here suggest that differences in BLL FA pair abundances should be applied with caution in field studies investigating viral infection.

To our knowledge, this is the first evidence of GlcADG in eukaryotic microalgae. It was found at roughly equivalent levels across all species (~1.61–5.91% of total polar lipids) except *P. gyrans*, where it was detected only at trace levels (Tables 2 and 3). Several of the dominant FA pairs detected in haptophytes (e.g., GlcADG 32:1, 34:1, and 34:2) have also been detected in SAR11 (Carini et al., 2015), making GlcADG less useful as a biomarker lipid for haptophytes.

4.2. Nitrogen limitation

E. huxleyi, *I. galbana*, and *P. parvum* shared a portion of conserved lipidomic response to N-limitation, all generating a significantly greater molecular diversity of TAGs, which we interpret as moving fixed carbon into chemical energy storage in TAGs instead of into N-demanding polar lipids (Supplementary Table S5). Previous analyses measured TAG accumulation under N-limitation in Pavlovales *Diacronema lutheri* (Guihéneuf and Stengel, 2013; Huang et al., 2020), and in Isochrysidales *Tisochrysis lutea* (Huang et al., 2019), where TAG synthesis resulted mostly from membrane lipid scavenging as opposed to de novo fatty acid synthesis. In contrast, Wang et al. (2015a,b) observed de novo TAG synthesis in *Isochrysis zhangjiangensis* under N-limitation, and both *E. huxleyi* CCMP 2090 and *T. lutea* have been shown to preferentially accumulate alkenones instead of TAG under N-limitation (da Costa et al., 2017; Bakku et al., 2018). These results suggest that the Isochrysidales have somewhat flexible carbon-storage responses to nitrogen starvation, and also that TAG accumulation may be a conserved lipidomic strategy under N-limitation for more recently diverged haptophytes.

P. parvum was able to mobilize a significant store of nitrogen by downregulating its most prominent polar lipid class, DGCC, and moderately upregulating PDPT. We also observed a large drop in relative abundance of glycolipids DGDG and SQDG, possibly indicating a reduction of the cell's photosynthetic machinery to a level that could be sustained by the low N availability, which is in agreement with documented reduced photosynthesis-related gene expression in N-limited *P. parvum* (Liu et al., 2015).

However, in contrast to the multifaceted responses in *I. galbana* and *P. parvum* to N-limitation, the only major polar lipid class change observed in *E. huxleyi* was a significant increase in sulfo-phospholipid PDPT, which, at over 10% of total polar lipids (Fig. 2; Table 4), became the most abundant non-plastidial membrane lipid. This increased PDPT expression in N-limited *E. huxleyi* has not been documented previously, and could have large-scale implications for oceanic DMS production, which is frequently found at elevated levels surrounding N-limited *E. huxleyi* blooms (Sunda et al., 2007; Wang et al., 2018). It is unclear how cells form PDPT, or whether its DMS moiety and extracellular DMS are biosynthetically related, and will necessitate future research.

Moreover, this novel lipidomic strategy of *E. huxleyi* under N limitation may be instrumental in their ability to form massive blooms. While upregulation of nutrient transporters and scavengers appears to be a logical, evolutionarily conserved response among nutrient-limited haptophytes (Dyhrman et al., 2006; Kang et al., 2007; Bruhn et al., 2010; Liu et al., 2015) and in nutrient-limited marine algae at large (Wurch et al., 2011; Dyhrman et al., 2012), lipid remodeling responses show high interspecific variability (Van Mooy et al., 2009; Cañavate et al., 2017b). Perhaps this element of phenotypic plasticity, and ability to utilize sulfur in membrane lipids, is a key attribute that enables *E. huxleyi* to form such preponderant blooms in oligotrophic ocean basins with low nitrate:phosphate ratios (Lessard et al., 2005). Interestingly, of all species in these analyses, only *H. ericina* shows equivalent PDPT concentrations to *E. huxleyi* under nutrient-replete conditions, presenting an intriguing possibility for future research.

In contrast, we saw no change to the relative composition of the polar lipidome of *P. gyrans*, except at trace levels. Huang et al. (2020) reported reduced abundance across all categories of membrane lipid in N-starved Pavlovales *D. lutheri*, and noted the non-plastidial membrane lipid and glycolipid compositions were not significantly different than in the control. Together, these results indicate more basal haptophytes may not have evolved equivalent headgroup replacement under N-limitation, and may instead indiscriminately recycle their lipid headgroups to free macronutrient reserves.

4.3. Phosphorus limitation

All four species show evidence of unique lipid remodeling strategies when P-limited, concomitant with metabolic processes investigated in previous research. However, *E. huxleyi, I. galbana,* and *P. parvum* all showed increased DGCC lipid fraction under P-limitation, suggesting the possibility of a conserved response.

In *P. parvum*, we observed small increases in the relative abundance of DGCC and GlcADG. The latter response has been documented in response to P-limitation in SAR11 (Carini et al., 2015) and higher plants (Okazaki et al., 2013).

P-limited *I. galbana* showed greater abundance of DGDG and an increased number of unique TAG molecules compared to the nutrient-replete culture, similar to recent research on another Isochrysidales *Tisochrysis lutea* (Huang et al., 2019), which observed increased de novo TAG synthesis. Though it has minimal constitutive phospholipids and little labile P storage in lipids to remodel for use under P-limitation (Cañavate et al., 2017a), *I. galbana* did exhibit an increase in DGCC, indicating the non-plastidial membrane fraction has increased slightly in relation to the plastidial membranes.

Surprisingly, we saw no significant lipidome changes between nutrient-replete and P-limited *P. gyrans*. Huang et al. (2020) observed maintenance of pigment content and growth rate in P-stressed Pavlovales *D. lutheri*, and struggled to achieve full P-limitation. Similarly, we may have struggled to achieve truly P-limited cultures of *P. gyrans*. However, *P. gyrans* contains minimal PG and undetectable PE and PC even under nutrient-replete conditions, limiting their ability to employ typical lipidomic strategies to mitigate P-limitation. These results, along with their limited response under N-limitation, suggest the broader cellular response of *P. gyrans* to nutrient limitation may be fundamentally different from other haptophytes.

Lipid class remodeling in *E. huxleyi* was limited in large part to DGCC, which rose to over 15% of polar lipids, and SQDG, which rose to almost 20%, reinforcing previous lipid analyses of *E. huxleyi* (Van Mooy et al., 2009; Shemi et al., 2016). BLL also doubled in relative expression, though the uncertainty around its true MS response factor and real abundance limits the inferences we can make as to its cellular importance. We did not observe statistically significant changes in the total pools of PG and PC, as reported by Shemi et al. (2016) and Van Mooy et al. (2009) in different strains of *E. huxleyi* than reported here, suggesting a more nuanced response to P-limitation by *E huxleyi* CCMP 374

than detected in studies of other strains.

Interestingly, changes in diagnostic ratios between non-phosphorus polar lipids and phospholipids were also not uniform, which may suggest that these ratios can be useful, but not sufficient, to diagnose P-limitation in the ocean. No species showed significant changes in SQDG:PG, and only *E huxleyi* showed a significant change in DGCC:PC ratio (Supplementary Fig. S6a). Cañavate et al. (2017b) also found somewhat less responsive betaine:phospholipid ratios in *I. galbana*. As they posit, this may be because, unlike *E. huxleyi*, these species are all adapted to relatively eutrophic, high N:P, coastal and estuarine habitats and contain minimal constitutive PC, thereby making lipids a non-viable source for labile P when limited.

However, the disparate responses to nutrient limitation reinforce the risk of overgeneralizing lipidomic nutrient-stress responses in phytoplankton, especially when the species in question have dissimilar lipidomes under replete conditions. They also present an intriguing possibility for further research: whether taxonomically divergent species with similar constitutive lipidomes (i.e., *E. huxleyi* and *P. globosa*; *I. galbana,* and *P. carterae*; Fig. 1) share a greater conserved response than taxonomically proximal species with disparate constitutive lipidomes (e.g., *I. galbana* and *E. huxleyi*).

Interestingly, the more recently diverged haptophytes in this study, *E. huxleyi*, *I. galbana,* and *P. parvum*, all in Class Prymnesiophyceae, appear to have conserved one remodeling strategy of increased relative abundance of DGCC under P-stress (Table 4), suggesting this ability may indeed be prevalent throughout the clade. In addition to enabling these algae to adapt to their environment, this response may have the capacity to alter the export and cycling into the mesopelagic and deep ocean—specifically, Fulton et al. (2017) and Kharbush et al. (2016) recently detected betaine lipids of apparent eukaryotic origin at 150 m in the North Atlantic and Sargasso Sea, and at 3000 m depth in the Tonga Trench, respectively, suggesting possible selective preservation and export of organic reduced-N to depth.

5. Conclusions

Haptophytes are a diverse and globally impactful clade of microalgae. Their prevalence and significant carbon content make them potent drivers of export, and their capacity for lipid remodeling ultimately influences the elemental composition of the community destined for export and remineralization. Elucidating the lipid fraction of these communities will therefore help us better understand export and remineralization processes in the ocean.

In this study, we cultured a diverse suite of haptophytes and analyzed their lipidomes under nutrient-replete conditions, as well as a subset of species under nitrogen and phosphorus limitation, finding unique lipidomes in each species with both common and divergent responses to nutrient stress. We identified a range of potential biomarkers for individual haptophyte species and, while we confirmed our hypothesis that each species would share a conserved portion of their lipidome, we were surprised by the extent to which their lipidomes diverged, potentially driven by relatively recent ecological adaptation. Also contrary to our hypothesis, we discovered unique lipidomic approaches to nutrient stress, especially with regards to *E. huxleyi* under N-limitation. Our findings highlight haptophyte lipidomic diversity and underline the importance of avoiding *a priori* conclusions of phenotypic or life-strategy generalization, even among closely related species.

Declaration of Competing Interest

The authors declare that they have no known competing financial interests or personal relationships that could have appeared to influence the work reported in this paper.

Acknowledgements

We thank S. Bent, H. Holm, and M. Jahns for their suggestions. We would also like to thank the Organic Geochemistry editorial staff and reviewers for their time and insightful feedback, which greatly improved the quality of the paper. This work was funded by a grant to B.A.S.V.M. from the Simons Foundation (#721229) and Gordon and Betty Moore Foundation (#5703). Support was also provided through grants to B.A.S.V.M. from the National Science Foundation (#17562524 and #2022597). Support for K.M. was provided by the U.K. Natural Environment Research Council in the form of a SPITFIRE Doctoral Training Partnership (# NE/L002531/1).

Data availability

All identified MS peak data and analysis code are available on the author's GitHub: https://github.com/PattonLowenstein/Haptophyte-Cultures.

Appendix A. Supplementary material

Supplementary data to this article can be found online at https://doi.org/10.1016/j.orggeochem.2021.104315.

References

Bakku, R.K., Araie, H., Hanawa, Y., Shiraiwa, Y., Suzuki, I., 2018. Changes in the accumulation of alkenones and lipids under nitrogen limitation and its relation to other energy storage metabolites in the haptophyte alga *Emiliania huxleyi* CCMP 2090. Journal of Applied Phycology 30, 23–36.

Beaufort, L., Couapel, M., Buchet, N., Claustre, H., Goyet, C., 2008. Calcite production by coccolithophores in the south east Pacific Ocean. Biogeosciences 5, 1101–1117.

Becker, K.W., Collins, J.R., Durham, B.P., Groussman, R.D., White, A.E., Fredricks, H.F., Ossolinski, J.E., Repeta, D.J., Carini, P., Armbrust, E.V., Van Mooy, B.A.S., 2018a. Daily changes in phytoplankton lipidomes reveal mechanisms of energy storage in the open ocean. Nature Communications 9, 5179.

Becker, K.W., Elling, F.J., Schröder, J.M., Lipp, J.S., Goldhammer, T., Zabel, M., Elvert, M., Overmann, J., Hinrichs, K.-U., 2018b. Isoprenoid quinones resolve the stratification of redox processes in a biogeochemical continuum from the photic zone to deep anoxic sediments of the Black Sea. Applied and Environment Microbiology 84, e02736–17.

Becker, K.W., Harke, M.J., Mende, D.R., Muratore, D., Weitz, J.S., DeLong, E.F., Dyhrman, S.T., Van Mooy, B.A.S., 2021. Combined pigment and metatranscriptomic analysis reveals highly synchronized diel patterns of phenotypic light response across domains in the open oligotrophic ocean. The ISME Journal 15, 520–533.

Benjamini, Y., Hochberg, Y., 1995. Controlling the false discovery rate: a practical and powerful approach to multiple testing. Journal of the Royal Statistical Society. Series B (Methodological) 57, 289–300.

Benner, I., Passow, U., 2010. Utilization of organic nutrients by coccolithophores. Marine Ecology Progress Series 404, 21–29.

Benton, H.P., Want, E.J., Ebbels, T.M.D., 2010. Correction of mass calibration gaps in liquid chromatography–mass spectrometry metabolomics data. Bioinformatics 26, 2488–2489.

Bigelow, N., Barker, J., Ryken, S., Patterson, J., Hardin, W., Barlow, S., Deodato, C., Cattolico, R.A., 2013. *Chrysochromulina* sp.: A proposed lipid standard for the algal biofuel industry and its application to diverse taxa for screening lipid content. Algal Research 2, 385–393.

Bligh, E.G., Dyer, W.J., 1959. A rapid method of total lipid extraction and purification. Canadian Journal of Biochemistry and Physiology 37, 911–917.

Bruhn, A., LaRoche, J., Richardson, K., 2010. *Emiliania huxleyi* (Prymnesiophyceae): nitrogen-metabolism genes and their expression in response to external nitrogen sources. Journal of Phycology 46, 266–277.

Cañavate, J.P., Armada, I., Hachero-Cruzado, I., 2017a. Aspects of phosphorus physiology associated with phosphate-induced polar lipid remodelling in marine microalgae. Journal of Plant Physiology 214, 28–38.

Cañavate, J.P., Armada, I., Hachero-Cruzado, I., 2017b. Interspecific variability in phosphorus-induced lipid remodelling among marine eukaryotic phytoplankton. New Phytologist 213, 700–713.

Carini, P., Van Mooy, B.A.S., Thrash, J.C., White, A., Zhao, Y., Campbell, E.O., Fredricks, H.F., Giovannoni, S.J., 2015. SAR11 lipid renovation in response to phosphate starvation. Proceedings of the National Academy of Sciences 112, 7767–7772.

Chambers, M.C., Maclean, B., Burke, R., Amodei, D., Ruderman, D.L., Neumann, S., Gatto, L., Fischer, B., Pratt, B., Egertson, J., Hoff, K., Kessner, D., Tasman, N., Shulman, N., Frewen, B., Baker, T.A., Brusniak, M.-Y., Paulse, C., Creasy, D., Flashner, L., Kani, K., Moulding, C., Seymour, S.L., Nuwaysir, L.M., Lefebvre, B., Kuhlmann, F., Roark, J., Rainer, P., Detlev, S., Hemenway, T., Huhmer, A., Langridge, J., Connolly, B., Chadick, T., Holly, K., Eckels, J., Deutsch, E.W.,

Moritz, R.L., Katz, J.E., Agus, D.B., MacCoss, M., Tabb, D.L., Mallick, P., 2012. A cross-platform toolkit for mass spectrometry and proteomics. Nature Biotechnology 30, 918–920.
Collins, J.R., Edwards, B.R., Fredricks, H.F., Van Mooy, B.A.S., 2016. LOBSTAHS: An adduct-based lipidomics strategy for discovery and identification of oxidative stress biomarkers. Analytical Chemistry 88, 7154–7162.
Conte, M., Volkman, J., Eglinton, G., 1994. Lipid biomarkers of the Haptophyta. In: Green, J.C., Leadbeater, B.S.C. (Eds.), The Haptophyte Algae, Clarendon Press, Oxford, pp. 351–377.
Cuvelier, M.L., Allen, A.E., Monier, A., McCrow, J.P., Messie, M., Tringe, S.G., Woyke, T., Welsh, R.M., Ishoey, T., Lee, J.-H., Binder, B.J., DuPont, C.L., Latasa, M., Guigand, C., Buck, K.R., Hilton, J., Thiagarajan, M., Caler, E., Read, B., Lasken, R.S., Chavez, F.P., Worden, A.Z., 2010. Targeted metagenomics and ecology of globally important uncultured eukaryotic phytoplankton. Proceedings of the National Academy of Sciences 107, 14679–14684.
da Costa, F., Le Grand, F., Quéré, C., Bougaran, G., Cadoret, J.P., Robert, R., Soudant, P., 2017. Effects of growth phase and nitrogen limitation on biochemical composition of two strains of *Tisochrysis lutea*. Algal Research 27, 177–189.
De Vargas, C., Aubry, M.-P., Probert, I., Young, J., 2007. Origin and evolution of coccolithophores: from coastal hunters to oceanic farmers. In: Evolution of Primary Producers in the Sea. Elsevier, pp. 251–285.
Dyhrman, S.T., Haley, S.T., Birkeland, S.R., Wurch, L.L., Cipriano, M.J., McArthur, A.G., 2006. Long serial analysis of gene expression for gene discovery and transcriptome profiling in the widespread marine coccolithophore *Emiliania huxleyi*. Applied and Environment Microbiology 72, 252–260.
Dyhrman, S.T., Jenkins, B.D., Rynearson, T.A., Saito, M.A., Mercier, M.L., Alexander, H., Whitney, L.P., Drzewianowski, A., Bulygin, V.V., Bertrand, E.M., Wu, Z., Benitez-Nelson, C., Heithoff, A., 2012. The transcriptome and proteome of the diatom *Thalassiosira pseudonana* reveal a diverse phosphorus stress response. PLoS ONE 7, 1–10.
Edvardsen, B., Eikrem, W., Throndsen, J., Sáez, A.G., Probert, I., Medlin, L.K., 2011. Ribosomal DNA phylogenies and a morphological revision provide the basis for a revised taxonomy of the Prymnesiales (Haptophyta). European Journal of Phycology 46, 202–228.
Fulton, J.M., Fredricks, H.F., Bidle, K.D., Vardi, A., Kendrick, B.J., DiTullio, G.R., Van Mooy, B.A.S., 2014. Novel molecular determinants of viral susceptibility and resistance in the lipidome of *Emiliania huxleyi*. Environmental Microbiology 16, 1137–1149.
Fulton, J.M., Fredricks, H.F., Van Mooy, B.A.S., 2017. Intact polar lipid export in the temperate western North Atlantic and Sargasso Sea. Organic Geochemistry 114, 45–56.
Guihéneuf, F., Stengel, D., 2013. LC-PUFA-enriched oil production by microalgae: accumulation of lipid and triacylglycerols containing n-3 LC-PUFA is triggered by nitrogen limitation and inorganic carbon availability in the marine haptophyte *Pavlova lutheri*. Marine Drugs 11, 4246–4266.
Guillard, R.R.L., Ryther, J.H., 1962. Studies of marine planktonic diatoms: I. *Cyclotella nana* Hustedt, and *Detonula confervacea* (Cleve) Gran. Canadian Journal of Microbiology 8, 229–239.
Guiry, M.D., Guiry, G.M., 2020. AlgaeBase [WWW Document]. AlgaeBase. URL https://www.algaebase.org (accessed 6.30.20).
Hakomori, S., 2008. Structure and function of glycosphingolipids and sphingolipids: recollections and future trends. Biochimica et Biophysica Acta - General Subjects 1780, 325–346.
Hennig, C., 2020. fpc: Flexible procedures for clustering.
Huang, B., Marchand, J., Thiriet-Rupert, S., Carrier, G., Saint-Jean, B., Lukomska, E., Moreau, B., Morant-Manceau, A., Bougaran, G., Mimouni, V., 2019. Betaine lipid and neutral lipid production under nitrogen or phosphorus limitation in the marine microalga *Tisochrysis lutea* (Haptophyta). Algal Research 40, 101506.
Huang, B., Mimouni, V., Lukomska, E., Bougaran, G., Morant-Manceau, A., 2020. Carbon partitioning and lipid remodeling during phosphorus and nitrogen starvation in the marine microalga *Diacronema lutheri* (Haptophyta). Journal of Phycology. https://doi.org/10.1111/jpy.12995.
Hunter, J.E., Frada, M.J., Fredricks, H.F., Vardi, A., Van Mooy, B.A.S., 2015. Targeted and untargeted lipidomics of *Emiliania huxleyi* viral infection and life cycle phases highlights molecular biomarkers of infection, susceptibility, and ploidy. Frontiers in Marine Science 2. https://doi.org/10.3389/fmars.2015.00081.
Juin, C., Bonnet, A., Nicolau, E., Bérard, J.-B., Devillers, R., Thiéry, V., Cadoret, J.-P., Picot, L., 2015. UPLC-MSE profiling of phytoplankton metabolites: application to the identification of pigments and structural analysis of metabolites in *Porphyridium purpureum*. Marine Drugs 13, 2541–2558.
Kang, L.-K., Hwang, S.-P.-L., Gong, G.-C., Lin, H.-J., Chen, P.-C., Chang, J., 2007. Influences of nitrogen deficiency on the transcript levels of ammonium transporter, nitrate transporter and glutamine synthetase genes in *Isochrysis galbana* (Isochrysidales, Haptophyta). Phycologia 46, 521–533.
Kharbush, J.J., Allen, A.E., Moustafa, A., Dorrestein, P.C., Aluwihare, L.I., 2016. Intact polar diacylglycerol biomarker lipids isolated from suspended particulate organic matter accumulating in an ultraoligotrophic water column. Organic Geochemistry 100, 29–41.
Kharbush, J.J., Close, H.G., Van Mooy, B.A.S., Arnosti, C., Smittenberg, R.H., Le Moigne, F.A.C., Mollenhauer, G., Scholz-Böttcher, B., Obreht, I., Koch, B.P., Becker, K.W., Iversen, M.H., Mohr, W., 2020. Particulate organic carbon deconstructed: molecular and chemical composition of particulate organic carbon in the ocean. Frontiers in Marine Science. https://doi.org/10.3389/fmars.2020.00518.
Kolde, R., 2019. pheatmap: Pretty Heatmaps.
Kuhl, C., Tautenhahn, R., Böttcher, C., Larson, T.R., Neumann, S., 2012. CAMERA: an integrated strategy for compound spectra extraction and annotation of liquid chromatography/mass spectrometry data sets. Analytical Chemistry 84, 283–289.
Laber, C.P., Hunter, J.E., Carvalho, F., Collins, J.R., Hunter, E.J., Schieler, B.M., Boss, E., More, K., Frada, M., Thamatrakoln, K., Brown, C.M., Haramaty, L., Ossolinski, J., Fredricks, H., Nissimov, J.I., Vandzura, R., Sheyn, U., Lehahn, Y., Chant, R.J., Martins, A.M., Coolen, M.J.L., Vardi, A., DiTullio, G.R., Van Mooy, B.A.S., Bidle, K. D., 2018. Coccolithovirus facilitation of carbon export in the North Atlantic. Nature Microbiology 3, 537–547.
Lessard, E.J., Merico, A., Tyrrell, T., 2005. Nitrate: phosphate ratios and *Emiliania huxleyi* blooms. Limnology and Oceanography 50, 1020–1024.
Li, Y., Lou, Y., Mu, T., Ke, A., Ran, Z., Xu, J., Chen, J., Zhou, C., Yan, X., Xu, Q., Tan, Y., 2017. Sphingolipids in marine microalgae: development and application of a mass spectrometric method for global structural characterization of ceramides and glycosphingolipids in three major phyla. Analytica Chimica Acta 986, 82–94.
Liu, H., Aris-Brosou, S., Probert, I., de Vargas, C., 2010. A time line of the environmental genetics of the haptophytes. Molecular Biology and Evolution 27, 161–176.
Liu, H., Probert, I., Uitz, J., Claustre, H., Aris-Brosou, S., Frada, M., Not, F., de Vargas, C., 2009. Extreme diversity in noncalcifying haptophytes explains a major pigment paradox in open oceans. Proceedings of the National Academy of Sciences 106, 12803–12808.
Liu, Z., Koid, A.E., Terrado, R., Campbell, V., Caron, D.A., Heidelberg, K.B., 2015. Changes in gene expression of *Prymnesium parvum* induced by nitrogen and phosphorus limitation. Frontiers in Microbiology 6. https://doi.org/10.3389/fmicb.2015.00631.
Marchetti, J., Bougaran, G., Dean, L.L., Mégrier, C., Lukomska, E., Kaas, R., Olivo, E., Baron, R., Robert, R., Cadoret, J.P., 2012. Optimizing conditions for the continuous culture of *Isochrysis affinis galbana* relevant to commercial hatcheries. Aquaculture 326–329, 106–115.
Martin, P., Dyhrman, S.T., Lomas, M.W., Poulton, N.J., Van Mooy, B.A.S., 2014. Accumulation and enhanced cycling of polyphosphate by Sargasso Sea plankton in response to low phosphorus. Proceedings of the National Academy of Sciences 111, 8089–8094.
Medlin, L.K., Sáez, A.G., Young, J.R., 2008. A molecular clock for coccolithophores and implications for selectivity of phytoplankton extinctions across the K/T boundary. Marine Micropaleontology 67 (1–2), 69–86. https://doi.org/10.1016/j.marmicro.2007.08.007.
Moore, C.M., Mills, M.M., Arrigo, K.R., Berman-Frank, I., Bopp, L., Boyd, P.W., Galbraith, E.D., Geider, R.J., Guieu, C., Jaccard, S.L., Jickells, T.D., La Roche, J., Lenton, T.M., Mahowald, N.M., Marañón, E., Marinov, I., Moore, J.K., Nakatsuka, T., Oschlies, A., Saito, M.A., Thingstad, T.F., Tsuda, A., Ulloa, O., 2013. Processes and patterns of oceanic nutrient limitation. Nature Geoscience 6, 701–710.
Müller, M., Trull, T., Hallegraeff, G., 2015. Differing responses of three Southern Ocean *Emiliania huxleyi* ecotypes to changing seawater carbonate chemistry. Marine Ecology Progress Series 531, 81–90.
Nichols, P.D., Skerratt, J.H., Davidson, A., Burton, H., McMeekin, T.A., 1991. Lipids of cultured *Phaeocystis pouchetii*: Signatures for food-web, biogeochemical and environmental studies in Antarctica and the Southern Ocean. Phytochemistry 30, 3209–3214.
Okazaki, Y., Otsuki, H., Narisawa, T., Kobayashi, M., Sawai, S., Kamide, Y., Kusano, M., Aoki, T., Hirai, M.Y., Saito, K., 2013. A new class of plant lipid is essential for protection against phosphorus depletion. Nature Communications 4, 1510.
Paasche, E., 2001. A review of the coccolithophorid *Emiliania huxleyi* (Prymnesiophyceae), with particular reference to growth, coccolith formation, and calcification-photosynthesis interactions. Phycologia 40, 503–529.
Popendorf, K.J., Fredricks, H.F., Van Mooy, B.A.S., 2013. Molecular ion-independent quantification of polar glycerolipid classes in marine plankton using triple quadrupole MS. Lipids 48, 185–195.
R Core Team, 2020. R: A language and environment for statistical computing. R Foundation for Statistical Computing, Vienna, Austria.
Ray, J.L., Haramaty, L., Thyrhaug, R., Fredricks, H.F., Van Mooy, B.A.S., Larsen, A., Bidle, K.D., Sandaa, R.-A., 2014. Virus infection of *Haptolina ericina* and *Phaeocystis pouchetii* implicates evolutionary conservation of programmed cell death induction in marine haptophyte–virus interactions. Journal of Plankton Research 36, 943–955.
Read, B.A., Klute, M.J., Kuo, A., Lefebvre, S.C., Maumus, F., Mayer, C., Miller, J., Monier, A., Salamov, A., Young, J., Aguilar, M., Claverie, J.-M., Frickenhaus, S., Gonzalez, K., Herman, E.K., Lin, Y.-C., Napier, J., Ogata, H., Sarno, A.F., Shmutz, J., Schroeder, D., de Vargas, C., Verret, F., von Dassow, P., Valentin, K., Van de Peer, Y., Wheeler, G., Dacks, J.B., Delwiche, C.F., Dyhrman, S.T., Glöckner, G., John, U., Richards, T., Worden, A.Z., Zhang, X., Grigoriev, I.V., 2013. Pan genome of the phytoplankton *Emiliania* underpins its global distribution. Nature 499, 209–213.
Rose, S.L., Fulton, J.M., Brown, C.M., Natale, F., Van Mooy, B.A.S., Bidle, K.D., 2014. Isolation and characterization of lipid rafts in *Emiliania huxleyi* : a role for membrane microdomains in host-virus interactions. Environmental Microbiology 16, 1150–1166.
Rost, B., Riebesell, U., 2004. Coccolithophores and the biological pump: responses to environmental changes. In: Thierstein, H.R., Young, J.R. (Eds.), Coccolithophores: From Molecular Processes to Global Impact. Springer Berlin Heidelberg, Berlin, pp. 99–125.
RStudio Team, 2020. RStudio: integrated development for R.
Sebastián, M., Smith, A.F., González, J.M., Fredricks, H.F., Van Mooy, B., Koblížek, M., Brandsma, J., Koster, G., Mestre, M., Mostajir, B., Pitta, P., Postle, A.D., Sánchez, P., Gasol, J.M., Scanlan, D.J., Chen, Y., 2016. Lipid remodelling is a widespread strategy in marine heterotrophic bacteria upon phosphorus deficiency. The ISME Journal 10, 968–978.

Shemi, A., Schatz, D., Fredricks, H.F., Van Mooy, B.A.S., Porat, Z., Vardi, A., 2016. Phosphorus starvation induces membrane remodeling and recycling in *Emiliania huxleyi*. New Phytologist 211, 886–898.
Smith, C.A., Want, E.J., O'Maille, G., Abagyan, R., Siuzdak, G., 2006. XCMS: processing mass spectrometry data for metabolite profiling using nonlinear peak alignment, matching, and identification. Analytical Chemistry 78, 779–787.
Sturt, H.F., Summons, R.E., Smith, K., Elvert, M., Hinrichs, K.-U., 2004. Intact polar membrane lipids in prokaryotes and sediments deciphered by high-performance liquid chromatography/electrospray ionization multistage mass spectrometry—new biomarkers for biogeochemistry and microbial ecology. Rapid Communications in Mass Spectrometry 18, 617–628.
Sunda, W.G., Hardison, R., Kiene, R.P., Bucciarelli, E., Harada, H., 2007. The effect of nitrogen limitation on cellular DMSP and DMS release in marine phytoplankton: climate feedback implications. Aquatic Sciences 69, 341–351.
Suzuki, R., Shimodaira, H., 2015. pvclust: hierarchical clustering with p-values via multiscale bootstrap resampling.
Tautenhahn, R., Böttcher, C., Neumann, S., 2008. Highly sensitive feature detection for high resolution LC/MS. BMC Bioinformatics 9, 504.
Van Mooy, B.A.S., Fredricks, H.F., Pedler, B.E., Dyhrman, S.T., Karl, D.M., Koblížek, M., Lomas, M.W., Mincer, T.J., Moore, L.R., Moutin, T., Rappé, M.S., Webb, E.A., 2009. Phytoplankton in the ocean use non-phosphorus lipids in response to phosphorus scarcity. Nature 458, 69–72.
Vardi, A., Haramaty, L., Van Mooy, B.A.S., Fredricks, H.F., Kimmance, S.A., Larsen, A., Bidle, K.D., 2012. Host-virus dynamics and subcellular controls of cell fate in a natural coccolithophore population. Proceedings of the National Academy of Sciences 109, 19327–19332.
Vardi, A., Van Mooy, B.A.S., Fredricks, H.F., Popendorf, K.J., Ossolinski, J.E., Haramaty, L., Bidle, K.D., 2009. Viral glycosphingolipids induce lytic infection and cell death in marine phytoplankton. Science 326, 861–865.
Vitousek, P.M., Aber, J.D., Howarth, R.W., Likens, G.E., Matson, P.A., Schindler, D.W., Schlesinger, W.H., Tilman, D.G., 1997. Human alteration of the global nitrogen cycle: sources and consequences. Ecological Applications 7, 737–750.
Volkman, J.K., 2016. Sterols in microalgae. In: Borowitzka, M.A., Beardall, J., Raven, J. A. (Eds.), The Physiology of Microalgae. Springer International Publishing, Cham, pp. 485–505.
Wagstaff, B.A., Rejzek, M., Field, R.A., 2018. Identification of a Kdn biosynthesis pathway in the haptophyte *Prymnesium parvum* suggests widespread sialic acid biosynthesis among microalgae. Journal of Biological Chemistry 293, 16277–16290.
Wakeham, S.G., 2020. Organic biogeochemistry in the oxygen-deficient ocean: A review. Organic Geochemistry 149, 104096.
Wakeham, S.G., Hedges, J.I., Lee, C., Peterson, M.L., Hernes, P.J., 1997. Compositions and transport of lipid biomarkers through the water column and surficial sediments of the equatorial Pacific Ocean. Deep Sea Research Part II: Topical Studies in Oceanography 44, 2131–2162.
Wakeham, S.G., Lee, C., 2019. Limits of our knowledge, part 2: Selected frontiers in marine organic biogeochemistry. Marine Chemistry 212, 16–46.
Wang, H.-T., Meng, Y.-Y., Cao, X.-P., Ai, J.-N., Zhou, J.-N., Xue, S., Wang, W., 2015a. Coordinated response of photosynthesis, carbon assimilation, and triacylglycerol accumulation to nitrogen starvation in the marine microalgae *Isochrysis zhangjiangensis* (Haptophyta). Bioresource Technology 177, 282–288.
Wang, S., Elliott, S., Maltrud, M., Cameron-Smith, P., 2015b. Influence of explicit *Phaeocystis* parameterizations on the global distribution of marine dimethyl sulfide. Journal of Geophysical Research, Biogeosciences 120, 2158–2177.
Wang, S., Maltrud, M., Elliott, S., Cameron-Smith, P., Jonko, A., 2018. Influence of dimethyl sulfide on the carbon cycle and biological production. Biogeochemistry 138, 49–68.
Wickham, H., Averick, M., Bryan, J., Chang, W., McGowan, L.D., François, R., Grolemund, G., Hayes, A., Henry, L., Hester, J., Kuhn, M., Pedersen, T.L., Miller, E., Bache, S.M., Müller, K., Ooms, J., Robinson, D., Seidel, D.P., Spinu, V., Takahashi, K., Vaughan, D., Wilke, C., Woo, K., Yutani, H., 2019. Welcome to the tidyverse. Journal of Open Source Software 4, 1686.
Wurch, L.L., Bertrand, E.M., Saito, M.A., Van Mooy, B.A.S., Dyhrman, S.T., 2011. Proteome changes driven by phosphorus deficiency and recovery in the brown tide-forming alga *Aureococcus anophagefferens*. PLoS ONE 6, 1–11.
Zapata, M., Jeffrey, S., Wright, S., Rodríguez, F., Garrido, J., Clementson, L., 2004. Photosynthetic pigments in 37 species (65 strains) of Haptophyta: implications for oceanography and chemotaxonomy. Marine Ecology Progress Series 270, 83–102.